BIOCHEMISTRY
including biophysical chemistry & molecular biology

Article

pubs.acs.org/biochemistry

# Role of *Rhodobacter sphaeroides* Photosynthetic Reaction Center Residue M214 in the Composition, Absorbance Properties, and Conformations of $H_A$ and $B_A$ Cofactors

Rafael G. Saer,[†] Amelia Hardjasa,[†] Federico I. Rosell,[‡] A. Grant Mauk,[‡] Michael E. P. Murphy,[†] and J. Thomas Beatty*[,†]

[†]Department of Microbiology and Immunology and [‡]Department of Biochemistry and Molecular Biology and Centre for Blood Research, The University of British Columbia, 2350 Health Sciences Mall, Vancouver, BC, Canada V6T 1Z3

Supporting Information

**ABSTRACT:** In the native reaction center (RC) of *Rhodobacter sphaeroides*, the side chain of (M)L214 projects orthogonally toward the plane and into the center of the A branch bacteriopheophytin (BPhe) macrocycle. The possibility that this side chain is responsible for the dechelation of the central $Mg^{2+}$ of bacteriochlorophyll (BChl) was investigated by replacement of (M)214 with residues possessing small, nonpolar side chains that can neither coordinate nor block access to the central metal ion. The (M)L214 side chain was also replaced with Cys, Gln, and Asn to evaluate further the requirements for assembly of the RC with BChl in the $H_A$ pocket. Photoheterotrophic growth studies showed no difference in growth rates of the (M)214 nonpolar mutants at a low light intensity, but the growth of the amide-containing mutants was impaired. The absorbance spectra of purified RCs indicated that although absorbance changes are associated with the nonpolar mutations, the nonpolar mutant RC pigment compositions are the same as in the wild-type protein. Crystal structures of the (M)L214G, (M)L214A, and (M)L214N mutants were determined (determined to 2.2−2.85 Å resolution), confirming the presence of BPhe in the $H_A$ pocket and revealing alternative conformations of the phytyl tail of the accessory BChl in the $B_A$ site of these nonpolar mutants. Our results demonstrate that (i) BChl is converted to BPhe in a manner independent of the aliphatic side chain length of nonpolar residues replacing (M)214, (ii) BChl replaces BPhe if residue (M)214 has an amide-bearing side chain, (iii) (M)214 side chains containing sulfur are not sufficient to bind BChl in the $H_A$ pocket, and (iv) the (M)214 side chain influences the conformation of the phytyl tail of the $B_A$ BChl.

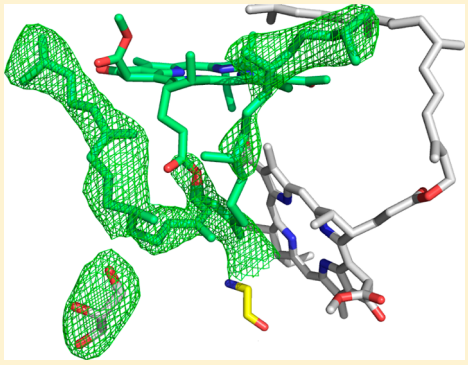

The photosynthetic reaction center (RC) of the alphaproteobacterium *Rhodobacter sphaeroides* is a transmembrane pigment−protein complex that is responsible for the trapping of light energy that drives electron transfer (ET) reactions, and the coupled formation of a proton gradient across the cytoplasmic membrane. High-resolution crystal structures of this RC revealed the organization of the three protein subunits, L, M, and H, which serve as a scaffold for the electronically active cofactors buried within the protein.[1,2] Cofactors are arranged in two symmetrical branches, A and B, of which only A is active in ET. The pigments consist of two electronically coupled bacteriochlorophylls ($P_A$ and $P_B$, together termed P), two accessory bacteriochlorophylls ($B_A$ and $B_B$), two bacteriopheophytins ($H_A$ and $H_B$), and two molecules of ubiquinone-10 ($Q_A$ and $Q_B$). These cofactors are arranged such that when P is promoted to an excited state, ET to an accessory pigment is the most rapid decay mechanism. Ultrafast visible and IR spectroscopic studies of the RC indicate that the primary electron acceptor is $B_A$, which is reduced on a time scale of ∼3 ps.[3,4] This $P^+B_A^-$ radical then reduces $H_A$ within 1 ps to generate the $P^+H_A^-$ state. The $H_A^-$ anion reduces $Q_A$ in ∼200 ps followed by ET to the $Q_B$ quinone in a reaction (∼200 μs) that is coupled to protonation of $Q_B$ to produce an electronically neutral ubisemiquinone radical.[5] A mobile cytochrome *c* reduces the oxidized $P^+$, and the RC is set for a second turnover in which the $Q_B$ ubisemiquinone is fully reduced to a quinol. This quinol is released from the RC and is oxidized at the cytochrome $b/c_1$ complex. The cytochrome $b/c_1$ complex reduces a mobile cytochrome *c*, resulting in a cyclic flow of electrons that is coupled to the translocation of a proton across the cytoplasmic membrane, and ATP synthesis.[6]

Studies of RC mutants have elucidated the importance of the protein component in fine-tuning the electronic properties of the pigments as well as the pigment composition of the RC.[3,7−10] Mutants have also allowed studies of protein−protein interactions involved in RC assembly[11,12] and the origin of the bacteriopheopytin (BPhe) in the $H_A$ and $H_B$ sites.[13,14] The biosynthetic pathway leading to bacteriochlorophyll (BChl) in bacteria such as *R. sphaeroides* is well-established, [15] and it is

**Received:** October 18, 2012
**Revised:** March 7, 2013
**Published:** March 12, 2013





dx.doi.org/10.1021/bi400207m | *Biochemistry* 2013, 52, 2206−2217

thought that BChl is the immediate precursor of BPhe.[16] Notably, the only known cellular location of BPhe is in the RC complex. Replacement of the axial Leu of the BPhe macrocycle with His resulted in the presence of BChl in place of BPhe in the $H_A$ and $H_B$ sites.[13,17,18] Conversely, replacing the axial His ligands of the P site BChls with nonpolar residues such as Leu, or Phe, resulted in BPhe instead of BChl at P.[13,19] A unifying hypothesis derived from these previous results is that key protein side chains that project toward the center of the chlorin macrocycle either bind (a His residue) or dechelate (a Leu or Phe residue) the BChl $Mg^{2+}$ and thereby determine whether BChl or BPhe is bound in a particular site within the RC.[13,14]

In this paper, we focus on the Leu residue at position 214 of the M subunit of the RC, (M)L214, and investigate the role of the protein component of the RC in (i) incorporation of BPhe versus BChl in the $H_A$ pocket, (ii) the efficiency of RC function, as indicated by cell culture growth rates under an extremely low photon flux, and (iii) influencing the conformation of the $B_A$ phytyl tail. These questions were addressed by replacing (M)L214 with Gly, Ala, Val, Ile, Met, Cys, Asn, Gln, or His. Aliphatic residues of varying volume were used to investigate the possibility that the absence of a bulky side chain at this position might result in the binding of BChl in the $H_A$ pocket. The sulfur- and amide-possessing residues were studied to determine whether these side chains would result in the incorporation of BChl in the $H_A$ pocket through coordination of $Mg^{2+}$ by sulfur, as in the $A_0$ chlorophyll of photosystem I,[20,21] or an amide oxygen, as in plant light-harvesting complex LHC-II.[22] The His substitution (M)L214H was included in this series as a control because this substitution had previously been shown to result in the presence of BChl in the $H_A$ pocket of the RC.[7] The consequences of these mutations were investigated by low-temperature electronic absorbance spectroscopy, light intensity-dependent cell growth kinetics, and X-ray crystallography.

## MATERIALS AND METHODS

**Bacterial Strains and Plasmids.** *R. sphaeroides* strain ΔRCLH and ΔpuhA were created as previously described.[11,23] Plasmid pRS1, containing a C-terminal hexahistidine tagged *puhA* and *pufQBALMX* genes required for photosystem expression under the hypoxia-induced *puc* promoter, was introduced into this strain by conjugation.[24] *R. sphaeroides* was grown semiaerobically in 2 L flasks at 30 °C in the dark, in 1.4 L of LB medium[25] supplemented with 810 μM $MgCl_2$, 510 μM $CaCl_2$, 1 mg/L thiamine hydrochloride, and 2 μg/mL tetracycline. *Escherichia coli* strain DH10B was used for cloning and site-directed mutagenesis, and cultivated in LB medium.

**Photoheterotrophic Growth Experiments.** For photoheterotrophic growth of *R. sphaeroides*, inoculum cultures were grown in RCV medium[26] aerobically on a rotary shaker at 200 rpm. Two hundred microliters of this culture was used to seed 16.5 mL photoheterotrophic starter cultures in screw cap tubes at 30 °C. These tubes were placed under a saturating light intensity for 48 h to adapt cells to photoheterotrophic conditions prior to low-light growth. Adapted cultures were transferred to fresh 16.5 mL screw cap tubes and diluted with RCV medium to a density of approximately 30 Klett units. Cultures were grown at a light intensity of 5 $\mu E\ m^{-2}\ s^{-1}$ [measured with an LI-185B photometer (Li-Cor)], and culture density measurements were taken with a Klett photoelectric colorimeter (100 Klett units ~ $3 \times 10^8$ CFU/mL).

**Mutagenesis and Cloning.** Plasmid pAli2::puf, containing the *pufQBALMX* genes of *R. sphaeroides*, was modified by site-directed mutagenesis using the primers listed in Table S1 of the Supporting Information. All mutagenic polymerase chain reaction (PCR) primer pairs were of the format 5′ CTCTA-CGGGTCGGCCXXXCTCTTCGCATGACAC 3′ (and the complement), where XXX denotes the codon for the Leu mutation. PCRs were performed in 50 μL reaction mixtures using 1 unit of Vent DNA Polymerase (NEB) in the presence of 5% DMSO and an additional 2 μL of a 50 mM $MgSO_4$ stock solution. The mutagenic PCR was performed with a 5 min initial denaturation at 95 °C, followed by 15 cycles of 95 °C for 20 s, 55 °C for 20 s, and 68 °C for 5.8 min. PCR tubes were added to the machine when it was heated to 85 °C, and the final extension step was conducted at 68 °C for 7 min. DpnI restriction endonuclease was added directly to the reaction mixture followed by incubation at 37 °C for 2 h prior to transformation of $CaCl_2$ competent *E. coli*. Mutations were confirmed by DNA sequencing.

The modified *pufQBALMX* operon was extracted from pAli2::puf by digestion with SacI and EcoRI, and this restriction fragment was subcloned into plasmid pRS2. The resultant plasmid was termed pRS1::(M)L214X, where X denotes the amino acid substitution.

**Purification of RCs.** Reaction centers were purified using a modified version of the protocol of Goldsmith and Boxer.[27] The cells from 21 L of the *R. sphaeroides* semiaerobic culture were collected by centrifugation, and the cell paste was resuspended in 10 mM Tris-HCl (pH 8.0), 150 mM NaCl, and 2 mM $MgCl_2$ to a volume of 175 mL. A few crystals of DNase I were added to the suspension before the cells were lysed in a French press at 18000 psi. Lysed cells were centrifuged to pellet debris and unbroken cells. The supernatant was then centrifuged at 66226*g* and 4 °C overnight to pellet chromatophores. Following ultracentrifugation, the supernatant was discarded and the remaining pellet was resuspended in 10 mM Tris (pH 8.0) and 150 mM NaCl to a volume of 100 mL. Samples (1 mL) of this suspension were placed in 1.7 mL microcentrifuge tubes and brought to room temperature, and lauryldimethylamine oxide [LDAO (Fluka)] was added to each tube at concentrations ranging from 0.5 to 2.75% to determine the optimal concentration of detergent for RC solubilization. These samples were rocked in the dark for 30 min, and 900 μL was centrifuged at 107400*g* for 30 min at 4 °C. The 875 nm absorbance maximum of the supernatants was used as a measure of the degree of photosynthetic complex solubilization. In our experiments, the optimal concentration of LDAO for chromatophore solubilization varied between 1.25 and 1.75%. Once the optimal LDAO concentration was found, the remaining chromatophore suspension was brought to this detergent concentration and stirred in the dark for 30 min at room temperature, and centrifuged at 117734*g* and 4 °C for 15 min. The supernatant solution was collected, and imidazole (10 mM) and NaCl (200 mM) were added to the indicated concentrations before the mixture was loaded onto a Ni NTA column (Qiagen). The column was washed with 10 mM Tris (pH 8.0), 150 mM NaCl, and 0.1% LDAO until the maximal absorbance over the range of 500−950 nm was less than 0.01. The RC was eluted from this column with 10 mM Tris (pH 8.0), 150 mM NaCl, 300 mM imidazole, and 0.1% LDAO and dialyzed against TL buffer [10 mM Tris (pH 8.0) and 0.1% LDAO]. For crystallization, RCs were purified further by anion exchange chromatography with an ÄKTA Explorer FPLC


dx.doi.org/10.1021/bi400207m | *Biochemistry* 2013, 52, 2206−2217

system (GE Healthcare) equipped with a SourceQ column and elution with a NaCl gradient (0 to 200 mM), with the majority of RCs eluting at 120 mM NaCl. The eluted RCs were desalted by being passed through a 10DG column (Bio-Rad) and concentrated with an Amicon 30 kDa centrifugal ultrafilter (Millipore). RCs used for crystallization experiments were not frozen and used immediately following purification.

**Pigment Quantification.** Pigments of RCs were extracted with a solution of acetone and methanol (7:2) and quantified according to the method of Van der Rest and Gingras.[28] Following the extraction, the samples were briefly centrifuged to remove a precipitate that formed upon addition of the organic solvent to the RC samples. Absorbance spectra of the isolated pigments were recorded on a Hitachi U-3010 spectrophotometer.

**X-ray Crystallography.** Fresh solutions of the RC purified as described above were used to set up hanging drop crystallization trials. Instead of mixing a reservoir solution with the protein, we prepared a separate precipitant solution [1 M potassium phosphate (pH 7.4), 3.5% 1,2,3-heptanetriol, and 0.1% LDAO] and mixed it with the protein solution on coverslips before sealing over the reservoir. Various ratios of precipitant and protein solution were found to result in crystals of widely varying quality. Diffraction quality crystals of (M)L214G (~0.3 mm × 0.3 mm × 0.3 mm) grew at a ratio of 2 $\mu$L of RC solution (7 mg/mL, or 20.6 $OD_{802}$/mL) to 1 $\mu$L of precipitant solution at 298 K, protected from light, over a reservoir of 1.52 M potassium phosphate buffer (pH 7.4). Crystals appeared after approximately 72 h. Repeated exposure of the crystals to light appeared to diminish diffraction quality, so immediately after the initial exposure to light, crystals were transferred to a solution of 1 M potassium phosphate buffer (pH 7.4) and 30% glycerol before being flash-frozen in liquid nitrogen. The (M)L214A and (M)L214N crystals were produced and frozen in a similar fashion, except that the former grew from a 5 mg/mL protein solution at a 3:1 protein:precipitant ratio and the (M)L214N crystals formed from a 3 mg/mL protein solution at a 2:1 drop ratio, over a reservoir of 1.5 M potassium phosphate buffer (pH 7.4).

Diffraction data from a single (M)L214G crystal were collected at the Canadian Light Source on beamline ID-1 and processed using AUTOXDS, Pointless, and Scala to 2.2 Å resolution.[29,30] Data sets for (M)L214A and (M)L214N crystals were collected at the Stanford Synchrotron Radiation Lightsource on beamline 7-1 and processed using HKL2000[31] for (M)L214A, or using Mosflm, Pointless, and Scala for (M)L214N.[30,32] All three mutant RCs crystallized in space group $P3_121$, with one molecule in the asymmetric unit. The solvent content was approximately 75%, which is typical for a membrane protein crystal. All data sets were isomorphous with the wild-type RC [PDB entry 2J8C, chosen for comparison because it is the highest-resolution (1.85 Å) RC structure in the PDB]. The (M)214 mutant structures initially underwent five cycles of rigid body refinement with Refmac5;[33] the input model used was an edited version of PDB entry 2J8C, with residue (M)L214 changed to the appropriate side chain. Subsequently, models were improved first by alternating between inspection of $2F_o - F_c$ and $F_o - F_c$ electron density maps and manual editing in Coot,[34] and followed by restrained refinement with Refmac5. Manual editing consisted primarily of adding and removing solvent molecules (mainly water, but also glycerol, 1,2,3-heptanetriol, and LDAO). Water molecules were added using >3$\sigma$ peaks in the $F_o - F_c$ difference map with plausible hydrogen bonding geometry. The restrained refinement used a geometry weighting term of 0.25, and the standard CCP4 library files were used for refinement of all cofactors.[35] To generate omit difference density maps, the occupancies of the phytyl tail atoms from CGA to C20, as well as LDAO and/or glycerol, were set to 0, and the model was refined by eight cycles of restrained refinement in Refmac5. Unweighted omit maps were generated using the FFT program in the CCP4 suite.[30] Data collection and refinement statistics are listed in Table 2.

**Low-Temperature Absorbance Spectroscopy.** Cryogenic absorbance spectra (0.6 nm bandwidth) were obtained at ~10−13 K using a Cary 6000 spectrophotometer (Agilent) equipped with a closed-cycle helium cryostat (Omniplex OM-8, ARS Inc.) as described by Lin et al.[36] RC samples in 10 mM Tris buffer (pH 8.0) and 0.1% LDAO were concentrated to an $A_{802}$ of ~40 by centrifugation using a 30 kDa cutoff Centricon ultrafilter (Millipore). Samples were supplemented with sodium ascorbate (final concentration of 1 mM) and diluted 1:1 with spectroscopic grade glycerol prior to being frozen between two quartz plates separated by an ~25 $\mu$m polycarbonate spacer.

## RESULTS

**Pigment Composition of (M)L214 Mutant RCs.** The BChl:BPhe ratios of all (M)L214 mutants were determined using organic solvent extracts of purified RCs and are listed in Table 1. These data indicate that RCs containing aliphatic or sulfur-containing side chains at (M)214 have a chlorin pigment composition that is the same as or close to that of the wild-type RC. Conversely, mutants with amide-containing side chains at $H_A$ (Asn and Gln) have a pigment composition that more closely resembles that of the previously reported (M)L214H mutant (i.e., five molecules of BChl for every molecule of BPhe).[7]

**Table 1. Calculated BChl:BPhe Ratios in Organic Solvent Extracts of WT and (M)L214 Mutant RCs[a]**

| | BChl:BPhe ratio |
|---|---|
| WT | 2.03 ± 0.09 |
| (M)L214G | 2.60 ± 0.11 |
| (M)L214A | 2.20 ± 0.11 |
| (M)L214C | 2.19 ± 0.09 |
| (M)L214V | 2.19 ± 0.02 |
| (M)L214I | 2.15 ± 0.11 |
| (M)L214M | 2.39 ± 0.01 |
| (M)L214H | 4.74 ± 0.04 |
| (M)L214N | 4.70 ± 0.29 |
| (M)L214Q | 4.77 ± 0.08 |

[a]Data are averages of three independent extractions ± the standard deviation of the mean.

**Effect of Replacement of (M)214 with Nonpolar or S-Containing Amino Acid Residues on the $Q_y$ and $Q_x$ Transitions of RC BPhes.** The 11 K electronic absorbance spectra of RC mutants bearing nonpolar residues at (M)214 are compared in Figure 1. At this temperature, spectroscopic differences that were subtle in room-temperature spectra (Figures S1 and S2 of the Supporting Information) became more evident. At ~760 nm, for example, the $Q_y$ transitions associated with the two BPhes in the wild-type RC overlapped considerably, although the absorbance on the red and blue edges of the peak corresponds to $H_A$ and $H_B$, respectively

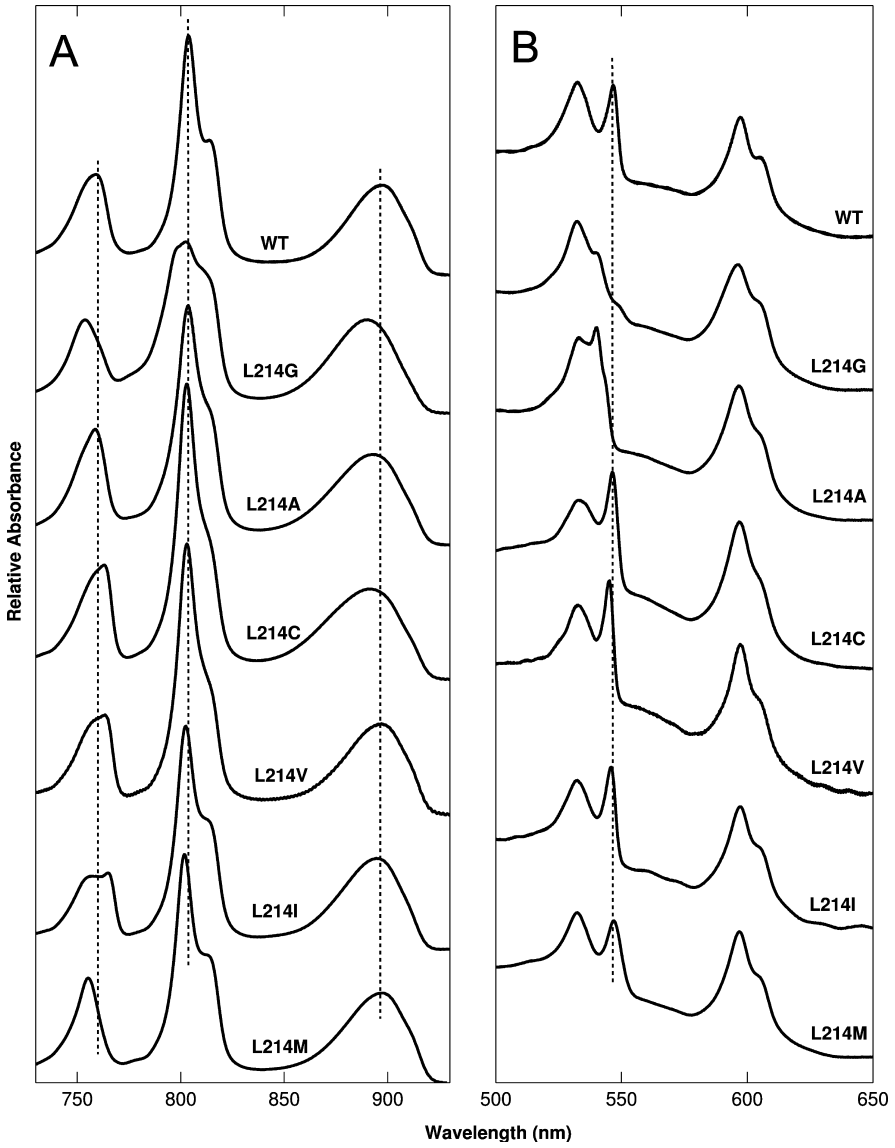


**Figure 1.** Low-temperature (~11 K) steady state absorption spectra of the (A) $Q_y$ and (B) $Q_x$ transitions of the nonpolar (M)214 mutant series. Spectra were normalized with respect to the $Q_y$ absorption maximum of the dimer (P) BChl peaks at ~895 nm. The dashed lines mark the $Q_x$ and $Q_y$ absorption peak wavelengths of $H_A$, as well as the peak wavelengths for the $Q_y$ transition of P and $B_A/B_B$, in the spectrum of the wild-type RC.

(Figure 1A).[37] All of the nonpolar (M)214 substitutions created in this work resulted in changes in the BPhe $Q_y$ absorbance region, ranging from almost imperceptible [in the (M)L214A RC] to most obvious in the (M)L214G, -I, and -M RCs. Replacement of (M)L214 with Gly resulted in a 5 nm blue shift of the BPhe $Q_y$ absorbance peak, from 759 to 754 nm, evidently due to a change in the $H_A$ band. In the spectra of the (M)L214M and (M)L214A mutants, the corresponding peak shifts were 3.9 and 0.4 nm, respectively. The overlap of the $H_A$ and $H_B$ $Q_y$ transitions was enhanced as a result, and the combined absorbance band appeared to be more symmetrical. In contrast, the absorbance spectra of the RC mutants with Cys, Val, or Ile in place of (M)L214 exhibited red shifts of the $H_A$ BPhe $Q_y$ transition maximum, thereby accentuating the resolution between the $Q_y$ absorbances of $H_A$ and $H_B$.

Together, the observations described above reflect primarily environmental perturbations of the $H_A$ chlorin when (M)L214 is replaced with another nonpolar residue, which affects the wavelength of light that is absorbed. Unlike the changes observed in the spectrum of the (M)L214H mutant (see below), the magnitudes of these shifts are much smaller, indicating that the pigment at this site was a BPhe in each mutant rather than a BChl.

As shown in Figure 1B, the low-temperature $Q_x$ transitions of the wild-type RC yielded three major absorbance peaks, and a long-wavelength shoulder. The peak near 535 nm is due to the $H_B$ BPhe, and the ~545 nm peak corresponds to the absorbance maximum of the $H_A$ BPhe; the peak and shoulder near 600 nm are due to BChls.[38,39]

The (M)L214G and (M)L214A RCs exhibited a blue shift of the $H_A$ BPhe peak, such that the two $Q_x$ transitions merge to form a peak with a shoulder (Figure 1B). In contrast, the BChl region around 600 nm was not greatly affected. These data confirm our interpretation of the $Q_y$ data: although the electronic properties of $H_A$ are affected when (M)L214 is substituted with small, nonpolar moieties such as Gly and Ala, the chlorin in the HA site remains a BPhe. The $H_B$ and $H_A$ $Q_x$ transitions of the (M)L214C, -V, -I, and -M mutants were


dx.doi.org/10.1021/bi400207m | *Biochemistry* 2013, 52, 2206−2217

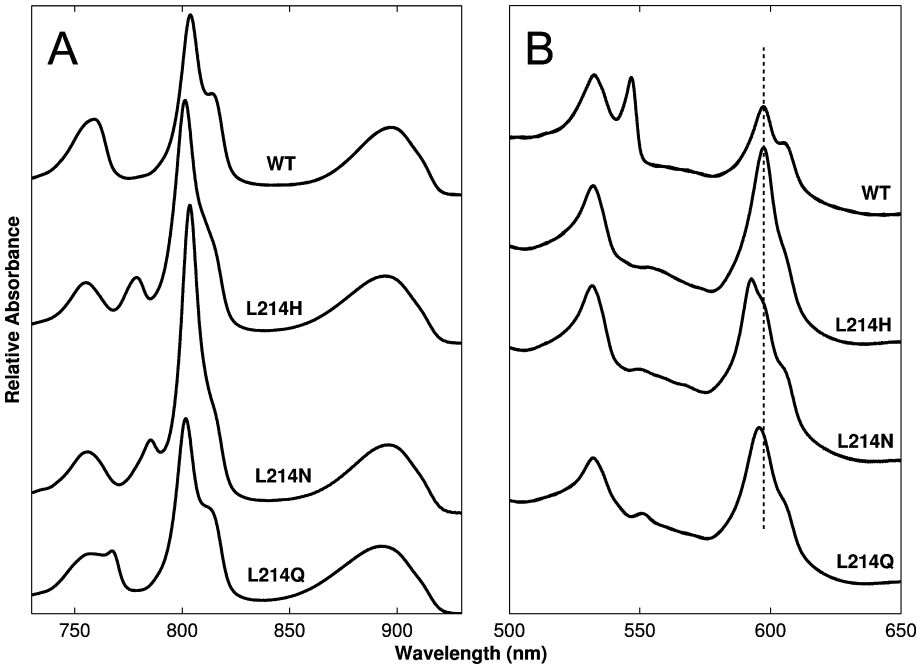


**Figure 2.** Low-temperature (~11 K) steady state absorption spectra of the (A) $Q_y$ and (B) $Q_x$ transitions of the polar (M)214 mutant series. Spectra were normalized with respect to the $Q_y$ absorption maximum of the dimer (P) BChl peaks at ~895 nm. The dashed line indicates the absorption peak wavelength of the BChl $Q_x$ transition in the spectrum of the wild-type RC.

relatively similar to each other, and to that of the wild-type RC, in peak amplitude and wavelength, indicating that the $H_A$ site of these mutants contains BPhe.

**Effect of Replacement of (M)214 with Nonpolar or S-Containing Amino Acid Residues on the $Q_y$ and $Q_x$ Transitions of RC BChls.** Because the (M)214 side chain is relatively distant from the RC BChl macrocycles, it was surprising to discover striking differences between the absorbance of wild-type and some nonpolar RCs in the ~802 nm $Q_y$ transition region of the $B_A/B_B$ accessory BChls. In the low-temperature absorbance spectrum of the wild-type RC, there is a major peak (attributed to a combination of $B_A$ and $B_B$) that has a distinct shoulder on the long-wavelength side, which has been attributed to the BChl in the inactive B branch ($B_B$).[39,40] It is interesting to note that the magnitude of this shoulder varies between low-temperature ground state absorbance spectra of the wild-type RC obtained by different groups.[41−43] In our work, the prominence of this shoulder was influenced by the bandwidth of the larger peak, which was correlated with the volume of the side chain at (M)214. RCs with nonpolar (M)214 side chains containing a $\delta$ or $\varepsilon$ carbon (Leu, Ile, or Met) exhibited a more pronounced shoulder than the (M)L214G, -A, -C, and -V RCs (Figure 1A). Note that in the case of the (M)L214C and (M)L214V RCs, the bandwidth increase of the larger, $B_A$ peak was accompanied by an increase in amplitude, in contrast to the (M)L214A RC, which showed no sign of amplitude increase (also see Figure S3 of the Supporting Information). The (M)L214G mutant is a special case, as the significantly broadened $B_A/B_B$ region appears to reveal an additional component at ~795 nm in addition to a large overall decrease in the amplitude of this region relative to that of the wild-type RC (Figure 1A and Figure S3 of the Supporting Information).

The $Q_y$ transitions of the P BChls of nonpolar mutants did not differ greatly. The P BChls in the (M)L214G mutant absorbed slightly to the blue compared to the wild-type RC. The (M)L214A and (M)L214C mutants also exhibited this change, although its magnitude was smaller than that of the (M)L214G mutant.

As for the $Q_x$ region, we focus on the overlapping ~595/605 nm peaks, which are composed of contributions from all BChl molecules present in the RC.[38] In contrast to the BPhe $Q_x$ region (~535/545 nm), the BChl $Q_x$ region was relatively unchanged (Figure 1B). Because the ~595/605 nm peaks were not greatly affected by the nonpolar mutations, relative to the ~535/545 nm peaks, the $Q_x$ absorbance data support the interpretations of the $Q_y$ data, that these mutations did not result in the presence of BChl in the $H_A$ pocket.

**The $Q_y$ and $Q_x$ Regions in the Absorbance Spectra of (M)214 Polar Mutants.** The 11 K absorbance spectra of the RC variants containing a polar residue at (M)214 differed significantly from the spectrum of the wild-type protein, resembling that of the "$\beta$-type" RC variant (M)L214H in important ways (Figure 2). For example, in the spectrum of the (M)L214N mutant, a new absorbance band was observed at 785 nm (denoted $\beta$), and the absorbance that remained at 756 nm decreased relative to the amplitude of the P BChl absorbance band. In other words, it appeared that the absorbance intensity associated with the $Q_y$ transition of a BPhe group was replaced with the corresponding absorbance of a new BChl group. In addition, there was an increase in the intensity of the $B_A$ BChl absorbance band of the (M)L214H and (M)L214N mutants, where the $\beta$ and $B_A$ absorbance bands overlap. In the case of the (M)L214Q RC, the relatively small red shift of the $H_A$ peak resulted in $B_A/B_B$ amplitudes similar to that of the wild-type RC (Figure S4 of the Supporting Information). Like the nonpolar and S-containing mutants [except (M)L214A and (M)L214G], these amplitude increases were also associated with a masking of the $B_B$ shoulder present in the $Q_y$ region of the spectrum.

The $Q_x$ transition spectra of the (M)L214N and (M)L214Q mutants confirm the conclusion that these RCs are $\beta$-type


dx.doi.org/10.1021/bi400207m | *Biochemistry* 2013, 52, 2206−2217

(Figure 2B). As in the (M)L214H control, the peak around 540 nm was absent from the absorbance spectra of the (M)L214N and (M)L214Q mutants, indicative of a loss of the $H_A$ BPhe from these RCs. There was a corresponding increase in the (M)L214H/Q RC absorbance around 595 nm, indicating the presence of BChl that was absent from the wild-type RC. Interestingly, the $Q_x$ region around 595 nm of the (M)L214N mutant was blue-shifted relative to those of the (M)L214H and -Q RCs.

In the wild-type RC, the BChl $Q_x$ region is composed of two components: a peak at ~595 nm, corresponding to the accessory $B_A$ and $B_B$ BChls, and a shoulder at ~605 nm, which represents the P BChls as well as a possible contribution from $B_A$.[38,39] In the (M)L214H mutant, the BChl $Q_x$ region had an increased amplitude at ~595 nm while retaining the ~605 nm shoulder [compare the relative magnitudes of the ~595 and ~535 nm peaks in the wild-type vs the (M)L2124H RC]. This $Q_x$ absorbance profile was thought to be representative of the additional BChl, and the corresponding loss of BPhe, at $H_A$.[7,44] However, in the amide-containing (M)L214N and -Q RCs, this ~595 nm peak was blue-shifted relative to those of the wild-type and (M)L214H mutant RCs. The shift was roughly 5 nm [(M)L214N] and ~1−2 nm [(M)L214Q]. Additionally, the polar mutant RCs exhibited a small absorbance peak at ~550 nm, most evident in the (M)L214Q RC spectrum, and absent from the wild-type and nonpolar RC mutant spectra [except perhaps as a minor feature in the (M)L214G RC spectrum (Figure 1B)].

**Photoheterotrophic Growth Rates.** The in vivo function of (M)214 mutant RCs was evaluated by comparing the RC-dependent phototrophic growth rates of strains containing RC mutations to an otherwise isogenic strain that contains the wild-type RC. Under the low photon flux used in this study (5 $\mu$E $m^{-2}$ $s^{-1}$), light intensity is a limiting growth factor, and cultures require a significantly longer time to reach the stationary phase than when grown under a high light intensity [~500 h vs ~50 h (data not shown)]. We postulated that under this low light intensity, RC performance in vivo may be measured indirectly as a phototrophic growth rate.

As shown in Figure 3, the control strain expressing the (M)L214H ($\beta$) mutant RC grew much more slowly than the strain containing the wild-type RC. It had been reported that (M)L214H mutant RCs are impaired in electron transfer because replacement of the $H_A$ BPhe with a BChl results in an increase in the free energy of the pigment by up to 300 meV, and a more positive midpoint potential.[7,44−46] Therefore, our in vivo measurement of culture growth rate under low light intensity corresponds to in vitro measurements of electron transfer rates in purified RCs. The growth of strains expressing the (M)L214N or (M)L214Q ($\beta$-like) mutant RCs was similarly impaired by comparison to strains expressing the wild type or the nonpolar or S-containing (M)214 mutants. These results indicate that the (M)L214N and (M)L214Q RCs are impaired with respect to electron transfer like the (M)L214H RC.

In contrast to the growth of the polar mutants, all of the strains containing nonpolar or S-containing substitutions at (M)214 grew with approximately the same kinetics as the wild-type strain (Figure 3). These similarities were surprising because the (M)L214G and -A mutants have been found to be impaired in terms of electron transfer from $H_A^-$ to $Q_A$, such that charge recombination competes with the forward reaction,

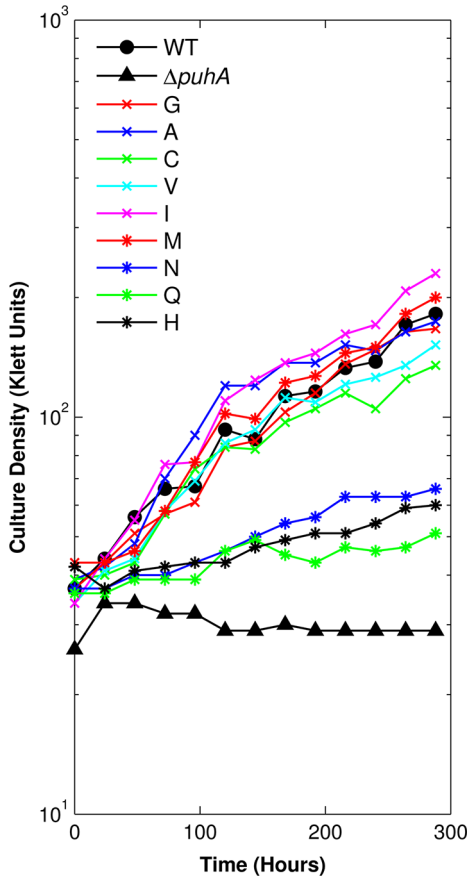


**Figure 3.** Photoheterotrophic growth of *R. sphaeroides* strains containing mutant RCs cultured with 5 $\mu$E $m^{-2}$ $s^{-1}$ illumination. The Δ*puhA* mutant, which lacks the RC H protein, illustrates zero growth. The single-letter amino acid code identifies the residue at (M)214 in the RC mutants. Curves are representative of three independent measurements.

resulting in a decrease in the overall yield of charge separation (Pan et al., manuscript submitted for publication).

**X-ray Crystal Structures.** The (M)L214G, (M)L214A, and (M)L214N mutants exhibited notable differences in their low-temperature absorbance spectra by comparison with those of the wild-type RC and each other (Figures 1 and 2). To identify structural changes in the RC, such as changes in the positions of $H_A$ and $B_A$, that might account for these spectroscopic changes, the crystal structures of these three mutant RCs were determined to resolutions of 2.20, 2.70, and 2.85 Å, respectively (Table 2). The protein backbones of all three mutant RCs were almost identical to that of the wild-type protein (PDB entry 2J8C, rmsds of <0.15 Å for all CA atoms).

In the crystal structures of the (M)L214G and (M)L214A mutant RCs, no difference from the wild-type RC in the location of the $H_A$ BPhe was observed within coordinate error. The $H_A$ chlorin was well-defined but lacked the electron density that would indicate a metal chelated in the macrocycle, consistent with the interpretation that the $H_A$ pocket contains a BPhe.

However, there were clear differences in electron density in the vicinity of (M)214 in addition to the mutations themselves. These differences were clearest in the highest-resolution structure of the (M)L214G mutant RC. In this structure, electron density around the phytyl tail of $B_A$ was discontinuous in the region where the tail bends, near the C4 methyl group

Table 2. X-ray Data Collection and Refinement Statistics for (M)L214G, (M)L214A, and (M)L214N RCs

| | (M)L214G | (M)L214A | (M)L214N |
|---|---|---|---|
| PDB entry | 4IN5 | 4IN6 | 4IN7 |
| unit cell parameters (Å) | | | |
| $a = b$ | 139.11 | 139.03 | 139.14 |
| $c$ | 184.69 | 184.34 | 185.14 |
| resolution (Å)[a] | 60.24−2.20 (2.32−2.20) | 60.00−2.70 (2.75−2.70) | 38.54−2.85 (3.00−2.85) |
| no. of reflections[b] | 579188 (105008) | 330265 (56265) | 353391 (48933) |
| $R_{merge}$[a] | 0.085 (0.590) | 0.154 (0.545) | 0.098 (0.498) |
| $I/\sigma I$[a] | 11.3 (2.8) | 25.7 (3.3) | 17.2 (4.3) |
| multiplicity[a] | 5.5 (5.4) | 5.9 (3.9) | 7.2 (7.3) |
| completeness[a] (%) | 99.9 (100.0) | 98.5 (97.8) | 99.9 (99.9) |
| $R_{work}$ | 0.191 | 0.189 | 0.179 |
| $R_{free}$ | 0.212 | 0.225 | 0.207 |
| Wilson $B$ factor (Å$^2$) | 38.8 | 53.2 | 60.9 |
| overall $B$ factor (Å$^2$) | 40.8 | 41.2 | 42.5 |
| rmsd for bond lengths (Å) | 0.018 | 0.019 | 0.020 |
| rmsd for bond angles (deg) | 1.91 | 2.18 | 2.27 |

[a]Numbers in parentheses reflect statistics for the highest-resolution shell. [b]The number in parentheses corresponds to the number of unique reflections.

(Figure 4A), implying that the $B_A$ tail is disordered. Notably, the bend in the phytyl tail is discernible and in the proximity of residue (M)L214 in the wild-type RC (Figure 4B). The volume made available by the deletion of the leucine side chain in the (M)L214G mutant RC is occupied in part by the rotation around the phytyl tail bend. By inspection of difference omit maps, the $B_A$ phytyl tail was modeled in two conformations with equal occupancy. The "right" conformer depicted in Figure 4A is equivalent to the conformation observed in the wild-type *R. sphaeroides* RC (Figure 4B). In the "left" conformation, also shown in Figure 4A, the $B_A$ phytyl tail is directed away from the $H_A$ macrocycle such that a portion of $H_A$ ring 1 is exposed to the solvent (see Discussion). In this conformer, the phytyl chain and a glycerol (cryoprotectant) molecule displace the molecule of LDAO detergent that occupies this space in the structure of the wild-type RC (compare panels A and B of Figure 4). The two conformers and glycerol molecule do not completely account for the difference density present in sigma-weighted and unweighted maps at the mutation site or in the region of the two phytyl tail conformations, suggesting that partially occupied solvent molecules and perhaps additional conformations of the phytyl tail are present. The difference maps derived from the (M)L214A crystal diffraction data are consistent with the two conformations of the phytyl tail (Figure 4C), although the lower quality of the (M)L214A data restricts structural comparisons with the (M)L214G structure to the mutation site.

In the (M)L214N crystal structure, positive difference electron density was obvious at the center of the chlorin macrocycle in the $H_A$ position (Figure 5). This density was modeled as a $Mg^{2+}$ ion, confirming that the chlorin at this position is a BChl group. After subsequent refinement, the $B$ factor associated with the $Mg^{2+}$ ion was commensurate with the BChl ring, and no residual difference density was present. At residue (M)214, adjacent to the $Mg^{2+}$, density for an Asn side chain was present and modeled accordingly. The (M)N214 OD2 atom is located approximately 2.0 Å from the $Mg^{2+}$; the $Mg^{2+}$ to OD2 bond angle is approximately perpendicular to the plane of the macrocycle, and the $Mg^{2+}$ ion is displaced ∼0.4 Å from the plane formed by the tetrapyrrole N atoms toward the new ligand, supporting the assignment of a metal−ligand bond. A similar ∼0.4 Å displacement of $Mg^{2+}$ from the plane was observed in the equivalent N−$Mg^{2+}$ bond between (L)H153 and the $B_A$ BChl (not shown). The ND1 atom of (M)N214 is within H-bond distance (3.1 Å) of the main chain carbonyl of (M)Y210. The alternative amide conformation of the Asn side chain with $Mg^{2+}$ coordination by the ND1 atom of Asn214 is unlikely because of the inability of the OD2 atom to establish a hydrogen bond with this main chain carbonyl group, and because of the requirement for the metal to displace a proton of the $NH_2$ group to form a metal−N ligand. Furthermore, the lone electron pair of the amide nitrogen atom should participate in a resonance structure of the amide group, resulting in a partial positive charge on the nitrogen.

## DISCUSSION

**Pigment Discrimination at $H_A$.** Our data support a hypothesis that the presence of BChl or BPhe in the $H_A$ pocket is determined solely by the presence or absence of an axial residue capable of $Mg^{2+}$ coordination. Although it was plausible that the RC $H_A$ pocket could dechelate a BChl $Mg^{2+}$ ion through steric exclusion via the bulky (M)L214 side chain, the absorbance spectra of RCs containing the (M)L214G and -A substitutions, which are neither bulky nor able to coordinate a $Mg^{2+}$ ion, resemble the wild-type spectrum more closely than the $\beta$ mutant spectrum. Furthermore, the crystal structures showed that the chlorin composition of the P, B, and H sites of the (M)L214G and -A RCs is the same as in the wild-type protein. Our results are complementary to and extend previous studies of "cavity mutants" of the *R. sphaeroides* RC, in which His axial ligands to the P BChls were changed to Gly residues, and proposed to introduce a cavity in the vicinity of the P BChls. Although crystal structures were not presented, Stark spectroscopy studies and pigment analysis demonstrated that those RCs assemble with a native pigment composition.[47] Furthermore, water molecules were proposed to act as a fifth ligand to the P BChls in the cavity mutants, and these waters appeared to be switched to other coordinating small molecules by incubation of the RC in the appropriate solute.[47] Our results with mutations at $H_A$ enrich our understanding of the complexity in pigment discrimination within RCs by indicating that not all binding pockets conform to a single set of rules

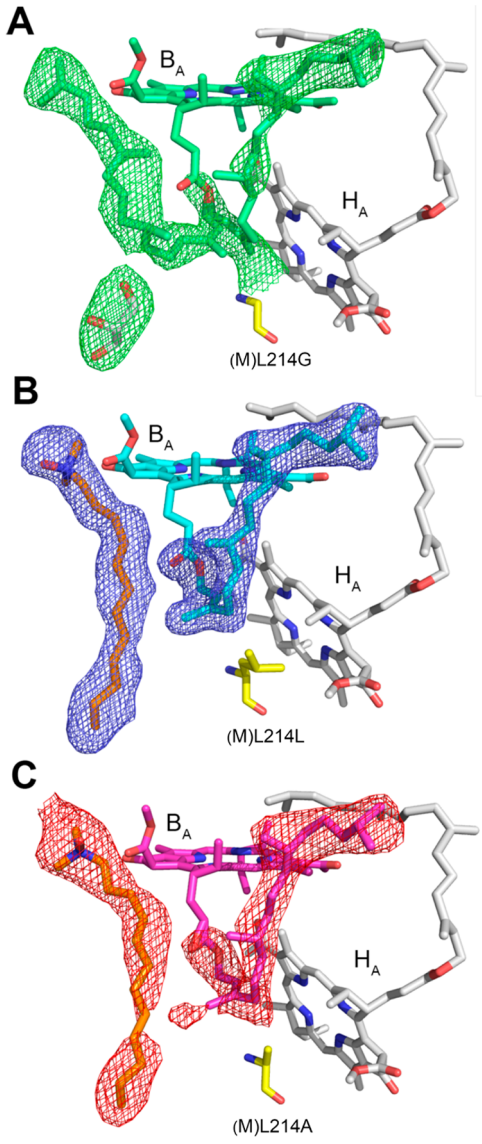


**Figure 4.** Omit difference electron density maps of (A) the (M)L214G RC, (B) the wild-type RC (PDB entry 2J8C), and (C) the (M)L214A RC. These maps were generated by setting the occupancy of the phytyl tail and the nearby LDAO (if present) to zero, followed by eight cycles of refinement. Discontinuous density is visible in the right conformation of the (M)L214G variant, and continuous density for the left conformation can also be seen. Electron density meshes are contoured at 3.0$\sigma$ and carved in a 2.5 Å radius. Oxygen atoms are colored red and nitrogen atoms blue. Carbon atoms are colored orange for LDAO, gray for glycerol and $H_A$, yellow for residue (M)214, and green, cyan, and magenta for the (M)L214G, wild-type, and (M)L214A RCs, respectively.

when it comes to populating these cofactor binding sites. Although adventitious ligands such as water may compensate for the loss of an imidazole group in the P BChls, such polar ligands do not appear to be suitable as BChl $Mg^{2+}$ ligands when the (M)214 Leu side chain is absent from the $H_A$ pocket. This difference may stem from the fact that the $H_A$ pocket is imbedded more deeply in the membrane bilayer than the P region and hence less likely to incorporate water.[48] Instead, the void is occupied in part by an alternative conformation of the phytyl tail of $B_A$. An analogous structural plasticity in the P region of the RC was found in "heterodimer" mutations in

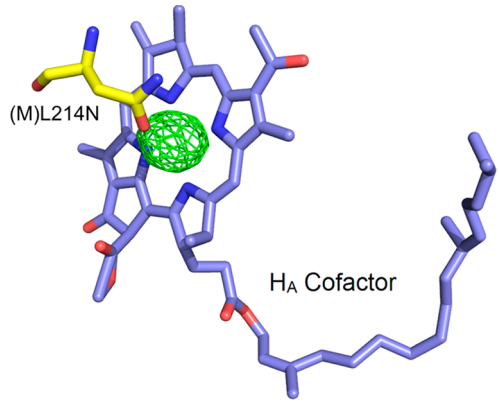


**Figure 5.** Omit difference electron density map of the (M)L214N RC, illustrating positive difference density for the $Mg^{2+}$ ion at the center of the chlorin ring of BChl in the $H_A$ site. The electron density mesh is contoured at 4.0$\sigma$ and carved in a 2.0 Å radius. Oxygen atoms are colored red and nitrogen atoms are blue. $H_A$ carbon atoms are colored purple and (M)L214N carbon atoms yellow.

which one of the P BChls was changed to BPhe by substitution of Leu for a His ligand to a BChl $Mg^{2+}$.[13,17] In an (M)L214H background, however, a heterodimer failed to assemble, and the resultant RC incorporated two BChls at P for unknown reasons.[44] Those results demonstrate that even when the coordinating axial (M)H202 residue is substituted with a Leu residue, the P binding pocket is capable of incorporating BChl. Although it is conceivable that an adventitious ligand was incorporated into the binding pocket of the P BChls [in the (M)H202/(M)L214H double mutant], those results raise additional questions about the nature of pigment selectivity in RCs as well as in the biogenesis of (B)Phes.

The biological production of a pheophytin (Phe) from a chlorophyll (Chl) is best understood in senescent plant materials. Shioi and co-workers partially purified a heat-stable "magnesium dechelating substance" that catalyzed the conversion of chlorophyllide to pheophorbide.[49] Although this as yet poorly defined low-molecular weight substance was implicated as functioning during leaf senescence, and therefore Chl degradation, the possibility that such a substance could function during Chl synthesis, to yield Phe for incorporation into RCs, cannot be excluded.

Other work on plant material, in this case the source of Phe in the photosystem II RC,[50] points to a pre-Chl origin of Phe in which a branch point in the Chl biosynthetic pathway appeared to yield Phe in etiolated leaves. The authors suggested that the magnesium chelatase enzyme itself was responsible for $Mg^{2+}$ removal.[50] Such a branch point has not been reported in the BChl biosynthesis pathway of purple phototrophic bacteria despite extensive mutagenic analyses.[15] Although it is possible that a dedicated dechelating enzyme exists for the synthesis of RC (B)Phe, a mutant strain deficient in this activity has not been discovered thus far. Moreover, (B)Phe is functionally present only in RCs, and free (B)Phe is not found in nonsenescent photosynthetic organisms. Alternatively, it is possible that the local environment of the (B)Phe-binding pockets within RCs, in general, results in the loss of $Mg^{2+}$ from (B)Chl unless a coordinating ligand specific for the central metal is present. Because of the tendency for this ion to exist only in the penta- or hexacoordinated state in BChl,[47,51,52] it is conceivable that the $Mg^{2+}$ is removed from the macrocycle in the $H_A$ site in part because of the absence of a fifth coordinate.


dx.doi.org/10.1021/bi400207m | *Biochemistry* 2013, 52, 2206−2217

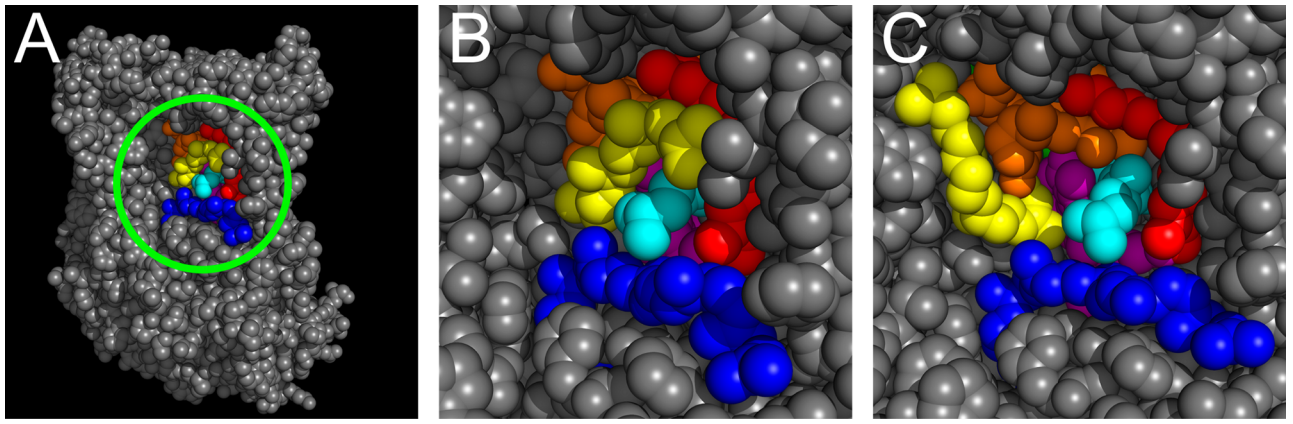


**Figure 6.** Organization of the pigment cofactors in crystal structures of the RC. (A) Overview of the wild-type RC (PDB entry 2J8C) with the region of interest enclosed by the green circle. (B) Close-up of the area indicated by the green circle in panel A. The phytyl and isoprenoid tails of the BChls, BPhe, and quinone on the A branch of the RC insulate electronically active pigment macrocycles by acting as a barrier against the external environment: cyan, $P_A$ tail; yellow, $B_A$ tail; orange, $B_A$ macrocycle; red, $H_A$ tail; magenta, $H_A$ macrocycle; blue, $Q_A$ tail; gray, protein. (C) View of the equivalent region highlighted in panel B, but in the (M)L214G mutant, with the $B_A$ phytyl tail modeled in the left orientation. The ring 1 acetyl group of the $H_A$ macrocycle (magenta) and ring 4 of the $B_A$ macrocycle (orange) are exposed to the RC external milieu.

**Spectroscopic and Structural Consequences of Nonpolar (M)L214 Mutations.** An interesting consequence of substituting (M)L214 with small-volume, nonpolar side chain residues in the *R. sphaeroides* RC is the shifting of the $Q_x$ transition corresponding to the $H_A$ BPhe to a higher energy. It was previously suggested by Bylina et al. that an analogous blue shift may be attributed to changes in the hydrogen bonding interaction between the $H_A$ BPhe macrocycle and a nearby Glu at position (L)104.[53] Specifically, when (L)E104 was changed to a weaker proton donor (Gln) or to another residue incapable of hydrogen bonding to the BPhe (Leu), the $Q_x$ absorbance maximum of $H_A$ became more similar to that of $H_B$. In the case of an RC (L)E104L mutant, the $Q_x$ transitions of $H_A$ and $H_B$ were almost overlapping. A similar blue shift was observed in our (M)L214G and (M)L214A mutants (Figure 2B), but the crystal structures show that these shifts are independent of changes in macrocycle hydrogen bonding interactions. We speculate that the changes in the $Q_x$ transition of $H_A$ observed in the (M)L214G and (M)L214A mutants are induced by the disorder in the $B_A$ phytyl tail, and related changes in the binding of detergent and possibly disordered water molecules.

Our X-ray structures of the (M)L214G and -A mutants reveal that this residue affects the orientation of the $B_A$ phytyl tail (Figure 4) and offer an explanation for the changes in the low-temperature absorbance spectra of the RCs with these low-volume side chains. Although the influence of the phytyl tail in the direct tuning of the electrochemical midpoint potential of a chlorin is not well understood and considered to be negligible, the tail was thought to affect the packing of nearby protein residues and other chlorins.[54] Our crystal structures indicate that, other than the substituted side chain itself, there is not a direct effect of the (M)214 side chain substitution on the electronic properties of $H_A$ (i.e., there appear to be no changes in the distance between the $H_A$ macrocycle and protein atoms that would give rise to changes in the electronic properties of the $H_A$ BPhe). Therefore, the absorbance changes in the $Q_x$ and $Q_y$ transitions of $H_A$ appear to stem predominantly from changes in the $B_A$ phytyl tail and perhaps disordered water, as an indirect effect of the substitution of (M)L214 with smaller, nonpolar moieties. These mutational changes are also accompanied by a broadening of the $Q_y$ absorbance band of $B_A$ in the (M)L214G mutant (Figure 1A), perhaps reflecting a population of mutant RCs that assume a range of alternative $B_A$ phytyl tail configurations, as indicated by the crystal structure.

Although the X-ray diffraction data from (M)L214A RC crystals indicate that some degree of $B_A$ phytyl tail disorder is present (Figure 4C), this disorder appears to be less than in the (M)L214G RC crystal, because electron density for the right conformation is continuous whereas electron density for the alternative conformation is weaker. It could be argued that this difference in electron density arises solely from the lower resolution of the (M)L214A data relative to the resolution of the data for the (M)L214G structure, but in the absorbance spectra, the broadening of the BChl $B_A$ $Q_y$ band is seen most prominently in the (M)L214G mutant (Figure 1A). To a lesser extent, the BChl $B_A$ $Q_y$ band is also broadened in the (M)L214A RC without a corresponding increase in the amplitude of the band (Figure S3 of the Supporting Information). In combination with the similarities between the (M)L214A and (M)L214G $Q_x$ transitions, these data indicate some disorder or motion in the (M)L214A $B_A$ phytyl tail, although it appears to be insufficient to allow the adoption of alternative conformations to the same degree as in the (M)L214G mutant.

The RC contains the electronically active cofactors within well-insulated tunneling pathways that prevent molecules such as intramembrane quinones from interacting with RC pigments and thus potentially affecting rates of electron transfer. In vivo, the RC is surrounded by light-harvesting complex 1 (LH1), which may act as a barrier between the quinone pool and the RC.[55−57] However, it was shown that 25−30% of the native quinone pool is retained in an isolated RC/LH1/PufX preparation,[58] evidently because quinones bind to these proteins and may be located within the space between the RC and LH1. In addition to the insulating shield provided by the RC protein matrix, the long, aliphatic phytyl tails esterified to the BChl and BPhe macrocycles may also serve a similar role, at least in vitro. This possibility becomes apparent when the RC crystal structure is viewed parallel to the plane of the membrane, along the side of the A branch, which reveals a cofactor-filled hole (Figure 6A). From this perspective, the phytyl tails of the BChls (yellow and cyan) and BPhes (red), as


dx.doi.org/10.1021/bi400207m | *Biochemistry* 2013, 52, 2206−2217

well as the isoprenoid tail of the $Q_A$ ubiquinone (blue), appear to insulate the macrocycles of $B_A$ (orange) and $H_A$ (magenta) from the external milieu (Figure 6B). However, our low-light intensity phototrophic growth experiments indicated that $B_A$ tail conformation heterogeneity does not have a great effect on the in vivo efficiency of RC function. Although it is plausible that these cofactor hydrophobic tails spontaneously adopt alternative configurations, there has been little account of the mechanisms by which these tails assume their native positions, or what factors might govern their three-dimensional configurations. However, the *R. sphaeroides* $B_A$ phytyl tail right configuration is conserved among all other type 2 RCs (Figure S5 of the Supporting Information).

The in vivo function of *R. sphaeroides* RCs containing these structural perturbations testifies to the robustness of this protein in the catalysis of light-driven excitation energy transduction. However, kinetic analysis of ET reactions in purified RCs reveals that the (M)L214G RC is significantly impaired in ET from $H_A$ to $Q_A$, as is the (M)L214A RC to a lesser extent (Pan et al., manuscript submitted for publication).

In contrast to the (M)L214G RC, the (M)L214C, (M)L214V, and (M)L214I RCs all exhibited red shifts of the $H_A$ $Q_y$ transition. It appears that the presence of a bulky moiety at position $\gamma$ of (M)214 (either SH in the case of Cys or two methyl groups in the case of Val and Ile) is sufficient to cause a detectable shift. Replacement of (M)L214 with Met has the opposite effect despite presenting a bulky moiety predicted to be at the same position as the Leu side chain in the wild-type RC. It is possible in the case of the (M)L214M mutant that the blue shift of the $H_A$ $Q_y$ transition stems from the establishment of hydrogen bonds between the Met residue SD atom and the pyrrole ring nitrogen protons of the BPhe macrocycle.

**Spectroscopic and Structural Consequences of Polar (M)L214 Mutations.** The mutant RCs containing Asn and Gln amide side chains at (M)214 incorporated BChl into the $H_A$ pocket. These proteins resemble the (M)L214H ($\beta$-type) mutant RC described by Kirmaier et al.[44] in terms of the in vivo activity indicated by similarly impaired phototrophic growth kinetics under a low light intensity (Figure 3). However, the absorbance band shifts induced by these three $\beta$-type mutations were very different from each other (Figure 2). Because the $Q_y$ band shifts of the (M)L214N and (M)L214Q RCs differed from each other more than from that of the (M)L214H RC (Figure 2A), we suggest that the absorbance spectra of $H_A$ BChls are not greatly affected by whether the $Mg^{2+}$-ligating atom is an imidazole nitrogen or an amide oxygen. In these cases, the possibility that the amide nitrogen atom acts as a ligand is excluded because of the participation of the nitrogen's lone electron pair in a resonance structure of the amide group, the location of the ND1 atom of (M)N214 within H-bonding distance of the main chain carbonyl of (M)Y210, and the need for loss of a proton of the $NH_2$ group to form a $Mg^{2+}$–N ligand.

The side chain of the residue replacing the Leu residue in the (M)L214N, (M)L214Q, and (M)L214H RCs differs in length and volume. The Asn side chain is shorter than the Gln side chain, but it offers equivalent atoms to coordinate the $Mg^{2+}$ ion. The (M)L214N and (M)L214Q RC $H_A$ $Q_y$ absorbance bands differed by ~25 nm (Figure 2A), so the length and/or volume of the $Mg^{2+}$-coordinating side chain appears to have a major effect on the energy of the $H_A$ $Q_y$ absorbance band, with the longer Gln side chain resulting in a higher-energy $H_A$ band in the $Q_y$ region. Indeed, studies of BChls in a variety of organic solvents demonstrated that the $Q_y$ transition is sensitive to the nature of the axial ligand to the pigment. Specifically, the $Q_y$ transition shifts to a higher energy when the $Mg^{2+}$ ion approaches the plane of the macrocycle because of a stronger metal–macrocycle interaction (this interaction being strongest in an in-plane $Mg^{2+}$, as is the case in hexacoordinated BChls), and vice versa.[59,60] The distance between the $H_A$ $Mg^{2+}$-coordinating atom in the (M)L214H side chain and the BChl $Mg^{2+}$ may be intermediate between the distances in the (M)L214N and (M)L214Q RCs; if so, this difference would account for the intermediate position of the $H_A$ $Q_y$ absorbance band relative the $H_A$ $Q_y$ bands of the (M)L214N and (M)L214Q RCs, but the coordinates of the (M)L214H mutant RC are unavailable.

On the basis of the available data, we suggest that the distance between the metal-coordinating atom of the RC protein and the $Mg^{2+}$ ion of (B)Chls, and therefore the position of the $Mg^{2+}$ relative to the plane of the (B)Chl macrocycle, is the major determinant of the $Q_y$ band energy in absorbance spectra, rather than the identity of the coordinating atom (i.e., a His nitrogen atom or an oxygen atom from Asn or Gln). Longer distances of coordinating atoms from the $Mg^{2+}$, as is the case with Asn, result in a $Q_y$ absorbance maximum at a longer wavelength, whereas shorter distances (as with His or Glu) result in correspondingly shorter wavelengths of $Q_y$ absorbance peaks.

The absorbance spectra and phototrophic growth rates of the mutants containing the (M)L214C or the (M)L214M RC indicate the presence of BPhe in the $H_A$ site, leading to the conclusion that sulfur-containing side chains are incapable of coordination to the $Mg^{2+}$ of a BChl at this position. Because the $Q_y$ band shifts of the (M)L214N, (M)L214Q, and (M)L214H RCs must reflect differences in $\beta_A$ excitation energies, these changes should be reflected in changes in ET rates, as in the original (M)L214H mutant RC.[44] Ongoing time-resolved spectroscopy and structural studies of all of the new mutants that we describe in this paper should yield a deeper understanding of connections between protein side chain composition, pigment content, and catalytic activity in this tractable experimental system.

## ■ ASSOCIATED CONTENT

### Supporting Information

Absorbance spectra of wild-type and nonpolar mutant RCs taken at room temperature (Figure S1), absorbance spectra of wild-type and polar mutant RCs taken at room temperature (Figure S2), overlay of the accessory BChl $Q_y$ transition of wild-type and (M)L214G, -A, -C, and -V mutant RCs from the 11 K absorbance spectra (Figure S3), overlay of the $Q_y$ transitions corresponding to the B and H regions in the absorbance spectrum of the WT and (M)L214H, -N, and -Q RCs (Figure S4), and orientation of the $B_A$ phytyl tails in RCs for which high-resolution data can be obtained (Figure S5). This material is available free of charge via the Internet at http://pubs.acs.org.

### Accession Codes

Data have been deposited as PDB entries 4IN5, 4IN6, and 4IN7.

## ■ AUTHOR INFORMATION

### Corresponding Author

*Phone: (604) 822-6896. E-mail: j.beatty@ubc.ca.

## Funding

J.T.B. and M.E.P.M. thank the Natural Sciences and Engineering Research Council of Canada (NSERC) for funding through the Discovery Grants system. R.G.S. thanks NSERC for a postgraduate fellowship. A.H. thanks CIHR for a Canadian Graduate Fellowship. The spectrophotometer and cryostat were funded by a Canada Foundation for Innovation Grant to A.G.M. Portions of the research described in this paper were performed at the Canadian Light Source, which is supported by the NSERC, the National Research Council Canada, the Canadian Institutes of Health Research, the Province of Saskatchewan, Western Economic Diversification Canada, and the University of Saskatchewan. Other portions of this research were conducted at the Stanford Synchrotron Radiation Lightsource (SSRL), a Directorate of SLAC National Accelerator Laboratory and an Office of Science User Facility operated for the U.S. Department of Energy Office of Science by Stanford University. The SSRL Structural Molecular Biology Program is supported by the U.S. Department of Energy Office of Biological and Environmental Research and by the National Institutes of Health, National Institute of General Medical Sciences (including Grant P41GM103393) and the National Center for Research Resources (Grant P41RR001209).


## Notes

The authors declare no competing financial interest.

## ■ ABBREVIATIONS

BChl, bacteriochlorophyll; BPhe, bacteriopheophytin; CFU, colony-forming units; Chl, chlorophyll; DMSO, dimethyl sulfoxide; LDAO, lauryl dimethylamine-*N*-oxide; PDB, Protein Data Bank; Phe, pheophytin; RC, reaction center; rmsd, root-mean-square deviation.

## ■ REFERENCES


(1) Allen, J. P., Feher, G., Yeates, T. O., Komiya, H., and Rees, D. C. (1987) Structure of the reaction center from *Rhodobacter sphaeroides* R-26: The protein subunits. *Proc. Natl. Acad. Sci. U.S.A. 84*, 6162−6166.

(2) Allen, J. P., Feher, G., Yeates, T. O., Komiya, H., and Rees, D. C. (1987) Structure of the reaction center from *Rhodobacter sphaeroides* R-26: The cofactors. *Proc. Natl. Acad. Sci. U.S.A. 84*, 5730−5734.

(3) Khatypov, R. A., Khmelnitskiy, A. Y., Khristin, A. M., Fufina, T. Y., Vasilieva, L. G., and Shuvalov, V. A. (2012) Primary charge separation within P870* in wild type and heterodimer mutants in femtosecond time domain. *Biochim. Biophys. Acta 1817*, 1392−1398.

(4) Pawlowicz, N. P., van Grondelle, R., van Stokkum, I. H., Breton, J., Jones, M. R., and Groot, M. L. (2008) Identification of the first steps in charge separation in bacterial photosynthetic reaction centers of *Rhodobacter sphaeroides* by ultrafast mid-infrared spectroscopy: Electron transfer and protein dynamics. *Biophys. J. 95*, 1268−1284.

(5) Paddock, M. L., Feher, G., and Okamura, M. Y. (2003) Proton transfer pathways and mechanism in bacterial reaction centers. *FEBS Lett. 555*, 45−50.

(6) Wraight, C. A. (2006) Chance and design: Proton transfer in water, channels and bioenergetic proteins. *Biochim. Biophys. Acta 1757*, 886−912.

(7) Kirmaier, C., Gaul, D., DeBey, R., Holten, D., and Schenck, C. C. (1991) Charge separation in a reaction center incorporating bacteriochlorophyll for photoactive bacteriopheophytin. *Science 251*, 922−927.

(8) Gibasiewicz, K., Pajzderska, M., Potter, J. A., Fyfe, P. K., Dobek, A., Brettel, K., and Jones, M. R. (2011) Mechanism of recombination of the $P^+H_A^-$ radical pair in mutant *Rhodobacter sphaeroides* reaction centers with modified free energy gaps between $P^+B_A^-$ and $P^+H_A^-$. *J. Phys. Chem. B 115*, 13037−13050.

(9) Mattioli, T. A., Lin, X., Allen, J. P., and Williams, J. C. (1995) Correlation between multiple hydrogen bonding and alteration of the oxidation potential of the bacteriochlorophyll dimer of reaction centers from *Rhodobacter sphaeroides*. *Biochemistry 34*, 6142−6152.

(10) Yakovlev, A. G., Vasilieva, L. G., Shkuropatov, A. Y., and Shuvalov, V. A. (2009) Primary processes of charge separation in reaction centers of YM210L/FM197Y and YM210L mutants of *Rhodobacter sphaeroides*. *Biochemistry (Moscow, Russ. Fed.) 74*, 1203−1210.

(11) Tehrani, A., and Thomas Beatty, J. (2004) Effects of precise deletions in *Rhodobacter sphaeroides* reaction center genes on steady-state levels of reaction center proteins: A revised model for reaction center assembly. *Photosynth. Res. 79*, 101−108.

(12) Tehrani, A., Prince, R. C., and Beatty, J. T. (2003) Effects of photosynthetic reaction center H protein domain mutations on photosynthetic properties and reaction center assembly in *Rhodobacter sphaeroides*. *Biochemistry 42*, 8919−8928.

(13) Bylina, E. J., and Youvan, D. C. (1988) Directed mutations affecting spectroscopic and electron transfer properties of the primary donor in the photosynthetic reaction center. *Proc. Natl. Acad. Sci. U.S.A. 85*, 7226−7230.

(14) Jaschke, P. R., and Beatty, J. T. (2007) The photosystem of *Rhodobacter sphaeroides* assembles with zinc bacteriochlorophyll in a bchD (magnesium chelatase) mutant. *Biochemistry 46*, 12491−12500.

(15) Willows, R. D., and Kriegel, A. M. (2009) Biosynthesis of bacteriochlorophylls in purple bacteria. In *The Purple Phototrophic Bacteria* (Hunter, C. N., Daldal, F., Thurnauer, M. C., and Beatty, J. T., Eds.) pp 57−79, Springer, Dordrecht, The Netherlands.

(16) Addlesee, H. A., and Hunter, C. N. (2002) *Rhodospirillum rubrum* possesses a variant of the bchP gene, encoding geranylgeranyl-bacteriopheophytin reductase. *J. Bacteriol. 184*, 1578−1586.

(17) Kirmaier, C., Holten, D., Bylina, E. J., and Youvan, D. C. (1988) Electron transfer in a genetically modified bacterial reaction center containing a heterodimer. *Proc. Natl. Acad. Sci. U.S.A. 85*, 7562−7566.

(18) Nabedryk, E., Schulz, C., Muh, F., Lubitz, W., and Breton, J. (2000) Heterodimeric versus homodimeric structure of the primary electron donor in *Rhodobacter sphaeroides* reaction centers genetically modified at position M202. *Photochem. Photobiol. 71*, 582−588.

(19) Schulz, C., Muh, F., Beyer, A., Jordan, R., Schlodder, E., and Lubitz, W. (1998) Investigation of *Rhodobacter sphaeroides* reaction center mutants with changed ligands to the primary donor. *Photosynthesis: Mechanisms and Effects*, Vol. *I*−*V*, pp 767−770, Springer, Dordrecht, The Netherlands.

(20) Jordan, P., Fromme, P., Witt, H. T., Klukas, O., Saenger, W., and Krauss, N. (2001) Three-dimensional structure of cyanobacterial photosystem I at 2.5 angstrom resolution. *Nature 411*, 909−917.

(21) Ben-Shem, A., Frolow, F., and Nelson, N. (2003) Crystal structure of plant photosystem I. *Nature 426*, 630−635.

(22) Kuhlbrandt, W., Wang, D. N., and Fujiyoshi, Y. (1994) Atomic model of plant light-harvesting complex by electron crystallography. *Nature 367*, 614−621.

(23) Chen, X. Y., Yurkov, V., Paddock, M. L., Okamura, M. Y., and Beatty, J. T. (1998) A *puhA* gene deletion and plasmid complementation system for facile site directed mutagenesis studies of the reaction center H protein of *Rhodobacter sphaeroides*. *Photosynth. Res. 55*, 369−373.

(24) Jaschke, P. R., Saer, R. G., Noll, S., and Beatty, J. T. (2011) Modification of the genome of *Rhodobacter sphaeroides* and construction of synthetic operons. *Methods Enzymol. 497*, 519−538.

(25) Sambrook, J., Fritsch, E. F., and Maniatis, T. (1989) *Molecular cloning: A laboratory manual*, 2nd ed., Cold Spring Harbor Laboratory Press, Plainview, NY.

(26) Beatty, J. T., and Gest, H. (1981) Generation of succinyl coenzyme-A in photosynthetic bacteria. *Arch. Microbiol. 129*, 335−340.

(27) Goldsmith, J. O., and Boxer, S. G. (1996) Rapid isolation of bacterial photosynthetic reaction centers with an engineered poly-histidine tag. *Biochim. Biophys. Acta 1276*, 171−175.

(28) Van der Rest, M., and Gingras, G. (1974) The pigment complement of the photosynthetic reaction center isolated from *Rhodospirillum rubrum*. *J. Biol. Chem. 249*, 6446−6453.
(29) Kabsch, W. (2010) Integration, scaling, space-group assignment and post-refinement. *Acta Crystallogr. D66*, 133−144.
(30) Winn, M. D., Ballard, C. C., Cowtan, K. D., Dodson, E. J., Emsley, P., Evans, P. R., Keegan, R. M., Krissinel, E. B., Leslie, A. G., McCoy, A., McNicholas, S. J., Murshudov, G. N., Pannu, N. S., Potterton, E. A., Powell, H. R., Read, R. J., Vagin, A., and Wilson, K. S. (2011) Overview of the CCP4 suite and current developments. *Acta Crystallogr. D67*, 235−242.
(31) Otwinowski, Z., and Minor, W. (1997) Processing of X-ray diffraction data. *Methods Enzymol. 276*, 307−326.
(32) Leslie, A. G. W., and Powell, H. R. (2007) Processing diffraction data with MOSFLM. *Methods Enzymol. 245*, 41−51.
(33) Murshudov, G. N., Vagin, A. A., and Dodson, E. J. (1997) Refinement of macromolecular structures by the maximum-likelihood method. *Acta Crystallogr. D53*, 240−255.
(34) Emsley, P., and Cowtan, K. (2004) Coot: Model-building tools for molecular graphics. *Acta Crystallogr. D60*, 2126−2132.
(35) Vagin, A. A., Steiner, R. A., Lebedev, A. A., Potterton, L., McNicholas, S., Long, F., and Murshudov, G. N. (2004) REFMAC5 dictionary: Organization of prior chemical knowledge and guidelines for its use. *Acta Crystallogr. D60*, 2184−2195.
(36) Lin, S., Jaschke, P. R., Wang, H., Paddock, M., Tufts, A., Allen, J. P., Rosell, F. I., Mauk, A. G., Woodbury, N. W., and Beatty, J. T. (2009) Electron transfer in the *Rhodobacter sphaeroides* reaction center assembled with zinc bacteriochlorophyll. *Proc. Natl. Acad. Sci. U.S.A. 106*, 8537−8542.
(37) Watson, A. J., Fyfe, P. K., Frolov, D., Wakeham, M. C., Nabedryk, E., van Grondelle, R., Breton, J., and Jones, M. R. (2005) Replacement or exclusion of the B-branch bacteriopheophytin in the purple bacterial reaction centre: The $H_B$ cofactor is not required for assembly or core function of the *Rhodobacter sphaeroides* complex. *Biochim. Biophys. Acta 1710*, 34−46.
(38) Shochat, S., Arlt, T., Francke, C., Gast, P., Vannoort, P. I., Otte, S. C. M., Schelvis, H. P. M., Schmidt, S., Vijgenboom, E., Vrieze, J., Zinth, W., and Hoff, A. J. (1994) Spectroscopic characterization of reaction centers of the (M)Y210W mutant of the photosynthetic bacterium *Rhodobacter sphaeroides*. *Photosynth. Res. 40*, 55−66.
(39) Kirmaier, C., Holten, D., and Parson, W. W. (1985) Picosecond-photodichroism studies of the transient states in *Rhodopseudomonas sphaeroides* reaction centers at 5 K. Effects of electron transfer on the 6 bacteriochlorin pigments. *Biochim. Biophys. Acta 810*, 49−61.
(40) Neupane, B., Jaschke, P., Saer, R., Beatty, J. T., Reppert, M., and Jankowiak, R. (2012) Electron transfer in *Rhodobacter sphaeroides* reaction centers containing Zn-bacteriochlorophylls: A hole-burning study. *J. Phys. Chem. B 116*, 3457−3466.
(41) Mattioli, T. A., Gray, K. A., Lutz, M., Oesterhelt, D., and Robert, B. (1991) Resonance raman characterization of *Rhodobacter sphaeroides* reaction centers bearing site-directed mutations at tyrosine M210. *Biochemistry 30*, 1715−1722.
(42) Middendorf, T. R., Mazzola, L. T., Lao, K. Q., Steffen, M. A., and Boxer, S. G. (1993) Stark-effect (electroabsorption) spectroscopy of photosynthetic reaction centers at 1.5K: Evidence that the special pair has a large excited-state polarizability. *Biochim. Biophys. Acta 1143*, 223−234.
(43) Frolov, D., Marsh, M., Crouch, L. I., Fyfe, P. K., Robert, B., van Grondelle, R., Hadfield, A., and Jones, M. R. (2010) Structural and spectroscopic consequences of hexacoordination of a bacteriochlorophyll cofactor in the *Rhodobacter sphaeroides* reaction center. *Biochemistry 49*, 1882−1892.
(44) Heller, B. A., Holten, D., and Kirmaier, C. (1995) Characterization of bacterial reaction centers having mutations of aromatic residues in the binding site of the bacteriopheophytin intermediary electron carrier. *Biochemistry 34*, 5294−5302.
(45) Fajer, J., Brune, D. C., Davis, M. S., Forman, A., and Spaulding, L. D. (1975) Primary charge separation in bacterial photosynthesis: Oxidized chlorophylls and reduced pheophytin. *Proc. Natl. Acad. Sci. U.S.A. 72*, 4956−4960.
(46) Cotton, T. M., and Vanduyne, R. P. (1979) An electrochemical investigation of the redox properties of bacteriochlorophyll and bacteriopheophytin in aprotic solvents. *J. Am. Chem. Soc. 101*, 7605−7612.
(47) Goldsmith, J. O., King, B., and Boxer, S. G. (1996) Mg coordination by amino acid side chains is not required for assembly and function of the special pair in bacterial photosynthetic reaction centers. *Biochemistry 35*, 2421−2428.
(48) Yeates, T. O., Komiya, H., Rees, D. C., Allen, J. P., and Feher, G. (1987) Structure of the reaction center from *Rhodobacter sphaeroides* R-26: Membrane-protein interactions. *Proc. Natl. Acad. Sci. U.S.A. 84*, 6438−6442.
(49) Shioi, Y., Tomita, N., Tsuchiya, T., and Takamiya, K. (1996) Conversion of chlorophyllide to pheophorbide by Mg-dechelating substance in extracts of *Chenopodium album*. *Plant Physiol. Biochem. 34*, 41−47.
(50) Ignatov, N. V., and Litvin, F. F. (1994) Photoinduced formation of pheophytin/chlorophyll-containing complexes during the greening of plant leaves. *Photosynth. Res. 42*, 27−35.
(51) Callahan, P. M., and Cotton, T. M. (1987) Assignment of bacteriochlorophyll *a* ligation state from absorption and resonance Raman spectra. *J. Am. Chem. Soc. 109*, 7001−7007.
(52) Evans, T. A., and Katz, J. J. (1975) Evidence for 5- and 6-coordinated magnesium in bacteriochlorophyll *a* from visible absorption spectroscopy. *Biochim. Biophys. Acta 396*, 414−426.
(53) Bylina, E. J., Kirmaier, C., Mcdowell, L., Holten, D., and Youvan, D. C. (1988) Influence of an amino-acid residue on the optical properties and electron transfer dynamics of a photosynthetic reaction centre complex. *Nature 336*, 182−184.
(54) Scheer, H. (2006) An overview of chlorophylls and bacteriochlorophylls: Biochemistry, biophysics, functions and applications. In *Chlorophylls and Bacteriochlorophylls* (Grimm, B., Porra, R. J., Rüdiger, W., and Scheer, H., Eds.), pp 1−26, Springer, Dordrecht, The Netherlands.
(55) Bahatyrova, S., Frese, R. N., Siebert, C. A., Olsen, J. D., Van Der Werf, K. O., Van Grondelle, R., Niederman, R. A., Bullough, P. A., Otto, C., and Hunter, C. N. (2004) The native architecture of a photosynthetic membrane. *Nature 430*, 1058−1062.
(56) Lilburn, T. G., Prince, R. C., and Beatty, J. T. (1995) Mutation of the Ser2 codon of the light-harvesting B870 alpha polypeptide of *Rhodobacter capsulatus* partially suppresses the *pufX* phenotype. *J. Bacteriol. 177*, 4593−4600.
(57) Qian, P., Bullough, P. A., and Hunter, C. N. (2008) Three-dimensional reconstruction of a membrane-bending complex: The RC-LH1-PufX core dimer of *Rhodobacter sphaeroides*. *J. Biol. Chem. 283*, 14002−14011.
(58) Comayras, R., Jungas, C., and Lavergne, J. (2005) Functional consequences of the organization of the photosynthetic apparatus in *Rhodobacter sphaeroides*. I. Quinone domains and excitation transfer in chromatophores and reaction center center dot antenna complexes. *J. Biol. Chem. 280*, 11203−11213.
(59) Fiedor, L., Kania, A., Mysliwa-Kurdziel, B., Orzel, L., and Stochel, G. (2008) Understanding chlorophylls: Central magnesium ion and phytyl as structural determinants. *Biochim. Biophys. Acta 1777*, 1491−1500.
(60) Hanson, L. K. (1988) Theoretical calculations of photosynthetic pigments. *Photochem. Photobiol. 47*, 903−921.